TECHNISCHE MECHANIK
an open access journal

journal homepage: www.ovgu.de/techmech

Tech. Mech., Vol. 40, Is. 2, (2020), 149–159

Received: 13.11.2019
Accepted: 20.05.2020
Available online: 27.05.2020

Longitudinal Fracture Analysis of an Inhomogeneous Stepped Rod with Two Concentric Cracks in Torsion

Victor Rizov[1]*, and Holm Altenbach[2]

[1] Department of Technical Mechanics, University of Architecture, Civil Engineering and Geodesy, 1 Chr. Smirnensky blvd., 1046 – Sofia, Bulgaria
[2] Lehrstuhl für Technische Mechanik, Fakultät für Maschinenbau, Otto-von-Guericke-Universität Magdeburg, Universitätsplatz 2, 39106 Magdeburg, Deutschland

Abstract: Analysis of the longitudinal fracture behaviour of an inhomogeneous stepped rod with two concentric longitudinal cracks is developed. The stepped rod has circular cross-section and exhibits continuous material inhomogeneity in radial direction. The material has non-linear elastic mechanical behaviour. The rod is subjected to torsion. The two cracks present concentric circular cylindrical surfaces. Thus, the fronts of the cracks are circles. The fracture is studied in terms of the strain energy release rate by considering the complementary strain energy stored in the rod. Solutions to the strain energy release rate are derived at different lengths of the two cracks. The balance of the energy is analyzed in order to verify the solutions. It is shown that the solutions can be applied also when the stepped rod is inhomogeneous in both radial and length directions. The solutions are used in order to evaluate the influences of the locations of the two concentric cracks in radial direction and the material inhomogeneity in radial and length directions on the longitudinal fracture behaviour of the stepped rod.

Keywords: longitudinal fracture behaviour, inhomogeneous stepped rod, two concentric longitudinal cracks

1 Introduction

One of the most important features of the load-bearing structural members and components exhibiting continuous (smooth) material inhomogeneity is the fact that the material properties are continuous functions of the coordinates (Tokovyy and Ma, 2008; Tokova et al., 2017; Tokovyy and Ma, 2013, 2016). The inhomogeneous structural materials present a great deal of interest for researchers mainly because certain kinds of inhomogeneous materials such as functionally graded materials have been increasingly used in various branches of practical engineering in the last three decades. Functionally graded materials are inhomogeneous composites manufactured by mixing of two or more constituent materials. Smooth spatial variation of material properties along one or more directions in the solid is obtained by continuously changing the microstructure of functionally graded materials during manufacturing. The fact that the material properties of functionally graded materials can be formed technologically in order to meet different performance requirements in different parts of a structural member is the basic advantage of functionally graded materials over the homogeneous structural materials (Altunsaray and Bayer, 2014; Jha et al., 2013; Knoppers et al., 2003; Mahamood and Akinlabi, 2017; Miyamoto et al., 1999; Nemat-Allal et al., 2011; Uysal and Kremzer, 2017; Uysal, 2016; Uysal and Güven, 2016). Therefore, functionally graded materials are frequently used in aeronautics, nuclear reactors, electronics and biomedicine.

Analysis of fracture behaviour plays a very important role in the design of inhomogeneous (functionally graded) structural members and components (Carpinteri and Pugno, 2006; Erdogan, 1995; Paulino, 2002; Tilbrook et al., 2005; Uysal and Güven, 2016).

Various works on fracture behaviour of linear-elastic composite materials with continuously inhomogeneous (functionally graded) composition have been reviewed in Tilbrook et al. (2005). Analyses of cracks oriented parallel or perpendicular to the direction of the material gradient have been considered. Investigations of failure resistance have also been discussed. Studies of fatigue fracture behaviour of functionally graded composites under cyclic crack loading conditions have been presented too. Different solutions for rectilinear cracks and also for arc cracks and slightly curved cracks in graded materials by applying methods of linear-elastic fracture mechanics have been summarized.

A method for evaluation of the strength of load-bearing functionally graded structures by using linear-elastic fracture mechanics has been developed in Carpinteri and Pugno (2006). Cracks and re-entrant corners have been analyzed. The influences of the varying corner angle and depth on the fracture have been analyzed assuming linear-elastic behaviour of the functionally graded material. It has been shown that the method is useful in engineering applications for predicting the strength of the structural members and components composed by functionally graded materials.

Fundamental problems of linear-elastic fracture mechanics of continuously inhomogeneous (functionally graded) materials and structures have been summarized and discussed in Erdogan (1995). The debonding of functionally graded coatings has been studied. Different aspects of surface fracture behaviour of functionally graded materials have been investigated and discussed in details.

It should be mentioned that certain kinds of inhomogeneous materials such as functionally graded materials can be built-up layer by layer (Mahamood and Akinlabi, 2017) which is a premise for appearance of longitudinal cracks between layers. Thus, longitudinal

* E-mail address: V_RIZOV_FHE@UACG.BG
doi: 10.24352/UB.OVGU-2020-022

fracture of inhomogeneous beam structures has been analyzed in a series of publications recently (Rizov, 2017; Rizov, 2018; Rizov, 2018).
In contrast to Rizov (2018) where an inhomogeneous circular shaft of a constant cross-section with one longitudinal crack under torsion is analyzed, the present paper deals with analysis of an inhomogeneous stepped rod of a circular cross-section with two concentric longitudinal cracks loaded in torsion. The stepped rod has non-linear elastic behaviour. It should be noted that the paper is motivated also by the fact that stepped rods loaded in torsion are widely used as components of various structures and mechanisms. Therefore, fracture analysis of stepped rods is an important research topic. In the present paper, the fracture is analyzed in terms of the strain energy release rate. Solutions to the strain energy release rate are derived by considering the complementary strain energy. The solutions are verified by analyzing the balance of the energy. The solutions are applied to evaluate the influence of the locations of the two cracks in radial direction and the material inhomogeneity on the longitudinal fracture behaviour of the stepped rod.

2 Calculation of the strain energy release rate

2.1 Calculation of the strain energy release rate by using the complementary strain energy

An inhomogeneous stepped rod with two longitudinal concentric cracks is shown in Fig. 1. In portions, PQ, QA and AD, the rod has circular cross-sections of radiuses R_1, R_2 and R_3, respectively. The lengths of rod portions PQ, QA and AD, are l_1, l_2 and $l-(l_1+l_2)$, respectively. The rod is clamped in section, D. The internal and external cracks are circular cylindrical surfaces of radiuses R_1 and R_2, respectively (Fig. 1). Thus, the fronts of the internal and external cracks are circles of radiuses R_1 and R_2, respectively. The lengths of the internal and external cracks are a_1 and a_2, respectively. In portion, QA, the rod is divided by the internal crack in internal and external part. The internal part is treated in the analysis as a rod of circular cross-section of radius R_1. The external part is treated as a ring-shaped rod of internal and external radiuses R_1 and R_2. In portion AB the rod is divided by the two cracks in three parts: internal, interstitial and external part. The internal part is treated in the analysis as a rod of circular cross-section of radius R_1. The interstitial part is treated as a ring-shaped rod of internal and external radiuses R_1 and R_2, respectively. The external part is treated as ring-shaped rod of internal and external radiuses R_2 and R_3, in portion AC. In the portion BC the rod is divided by the external crack in two parts: internal and external part. The internal part is treated as a rod of circular cross-section of radius R_2 and length a_2-a_1. The rod is loaded in torsion by three torsion moments T_1, T_2 and T_3 applied, respectively, in cross-sections P, Q and A, as shown in Fig. 1. The rod exhibits continuous (smooth) material inhomogeneity in radial direction. The material has non-linear elastic behaviour.
The longitudinal fracture is analyzed in terms of the strain energy release rate. For this purpose, first, an elementary increase $\mathrm{d}a_1$ of the length of the internal crack is assumed and the strain energy release rate G_{a_1} is expressed as (Rizov, 2018)

$$G_{a_1}=\frac{\mathrm{d}U^*}{l_{\mathrm{cf1}}\mathrm{d}a_1} \tag{1}$$

where U^* is the complementary strain energy stored in the beam and l_{cf1} is the length of the front of the internal crack. Since

$$l_{\mathrm{cf1}}=2\pi R_1, \tag{2}$$

Eq. (1) is re-written as

$$G_{a_1}=\frac{\mathrm{d}U^*}{2\pi R_1\mathrm{d}a_1}. \tag{3}$$

The complementary strain energy is obtained as

$$U^*=U^*_{\mathrm{IN1}}+U^*_{\mathrm{IS1}}+U^*_{\mathrm{EX}}+U^*_{\mathrm{IN2}}+U^*_{\mathrm{CD}}, \tag{4}$$

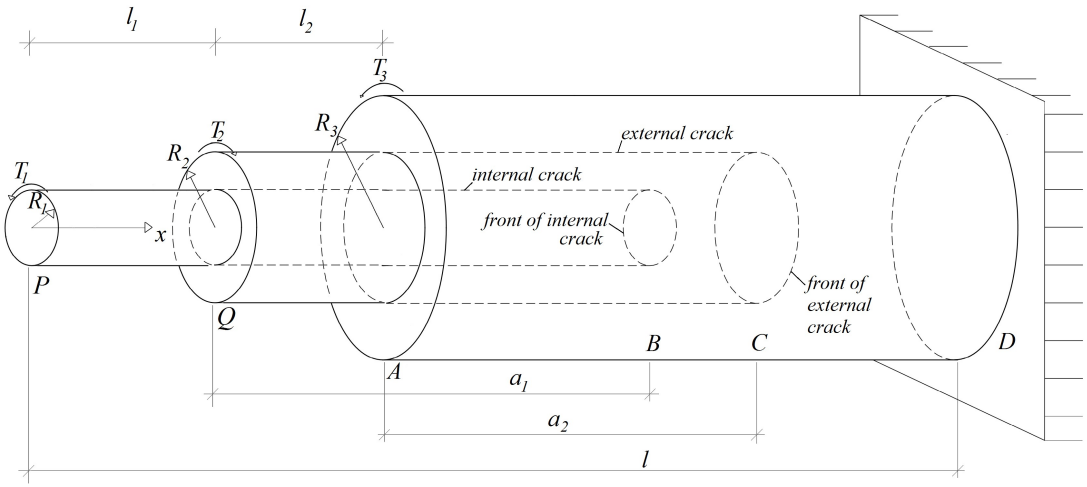

Fig. 1: Geometry and loading of an inhomogeneous stepped rod with two concentric longitudinal cracks

where U^*_{IN1} the complementary strain energy in the rod portion PQ and in the internal parts of portions QA and AB of the rod, U^*_{IS1} is the complementary strain energy in the external part of the rod portion QA and in the interstitial part of the portion AB of the rod, U^*_{EX} is the complementary strain energy in the external part of portion AC of the rod, U^*_{IN2} is the complementary strain energy in the internal part of portion BC of the rod, U^*_{CD} is the complementary strain energy in the un-cracked portion CD of the rod. The complementary strain energy in the rod portion PQ and in the internal parts of portions QA and AB of the rod is expressed as

$$U^*_{\mathrm{IN1}} = \int_0^{l_1+a_1} \int_0^{R_1} \int_0^{2\pi} u^*_{0\mathrm{IN1}} R \mathrm{d}x \mathrm{d}R \mathrm{d}\varphi, \tag{5}$$

where $u^*_{0\mathrm{IN1}}$ is the complementary strain energy density, R and φ are the polar coordinates, x is the longitudinal centroidal axis of the rod. The complementary strain energy density is calculated by using the following formula (Rizov, 2018):

$$u^*_{0\mathrm{IN1}} = \tau\gamma - u_{0\mathrm{IN1}}, \tag{6}$$

where τ is the shear stress, γ is the shear strain, $u_{0\mathrm{IN1}}$ is the strain energy density. In principle, the strain energy density is equal to the area enclosed by the stress-strain diagram. Thus, $u_{0\mathrm{IN1}}$ is expressed as

$$u_{0\mathrm{IN1}} = \int_0^{\gamma} \gamma\tau(\gamma)\mathrm{d}\gamma. \tag{7}$$

In the present paper, the mechanical behaviour of the material is treated by applying the following non-linear stress-strain relation (Lukash, 1998):

$$\tau = \frac{G\gamma}{\sqrt{1+\gamma^2}}, \tag{8}$$

where G is the shear modulus. By substituting of (8) in (7), one obtains

$$u_{0\mathrm{IN1}} = G\left(\sqrt{1+\gamma^2} - 1\right). \tag{9}$$

The complementary strain energy density is found by substituting of (8) and (9) in (6)

$$u^*_{0\mathrm{IN1}} = G\left(1 - \frac{1}{\sqrt{1+\gamma^2}}\right). \tag{10}$$

The rod exhibits continuous material inhomogeneity in radial direction. Thus, the distribution of G in radial direction is treated by using an exponential law

$$G = G_0 \mathrm{e}^{p\frac{R}{R_3}}, \tag{11}$$

where

$$0 \le R \le R_3. \tag{12}$$

In (11) G_0 is the value of G in the centre of the cross-section of the rod, p is a material property that controls the material inhomogeneity in radial direction.
The distribution of the shear strain in radial direction is treated by applying the Bernoulli's hypothesis for plane sections since rods of a high length to diameter ratio are under consideration in the present paper. Thus, the distribution of γ in the cross-section of the rod portion PQ and in the internal parts of portions QA and AB of the rod is written as

$$\gamma = \gamma_{\mathrm{m}} \frac{R}{R_1}, \tag{13}$$

where

$$0 \le R \le R_1. \tag{14}$$

In (13) γ_{m} is the shear strain at the periphery of the rod portion PQ and at the periphery of the internal parts of portions QA and AB of the rod. The following equation for equilibrium of the elementary forces in the cross-section is used to determine γ_{m}:

$$T_1 = \int_0^{R_1} \int_0^{2\pi} \tau R^2 \mathrm{d}R\mathrm{d}\varphi \tag{15}$$

After substituting of (8), (11) and (13) in (15), the equation for equilibrium is solved with respect to γ_{m} by using the MatLab computer program.

The complementary strain energy in the external part of the rod portion QA and in the interstitial part of portion AB of the rod (Fig. 1)

$$U^*_{\mathrm{IS1}} = \int_0^{l_1+a_1} \int_0^{R_1} \int_0^{2\pi} u^*_{0\mathrm{IS1}} R\mathrm{d}x\mathrm{d}R\mathrm{d}\varphi, \tag{16}$$

where $u^*_{0\mathrm{IS1}}$ is the complementary strain energy density. Equation (10) is applied to derive $u^*_{0\mathrm{IS1}}$. For this purpose, γ is replaced with γ_{IN1}. The distribution of shear strain γ_{IN1} is expressed as

$$\gamma_{\mathrm{IN1}} = \gamma_{\mathrm{mIN1}} \frac{R}{R_2}, \tag{17}$$

where

$$R_1 \leq R \leq R_2. \tag{18}$$

In (10) γ_{mIN1} is the shear strain at the periphery of the rod portion QA and at the periphery of the interstitial part of portion AB of the rod. The following equation for equilibrium is used to derive γ_{mIN1} (Fig. 1):

$$T_2 = \int_{R_1}^{R_2} \int_0^{2\pi} \tau_{\mathrm{IN1}} R^2 \mathrm{d}R\mathrm{d}\varphi, \tag{19}$$

where the distribution of the shear strain τ_{IN1} is found by replacing of γ with γ_{IN1} in Eq. (8). After substituting of τ_{IN1} in (19), the equation for equilibrium is solved with respect to τ_{mIN1} by the MatLab computer program.
The complementary strain energy U^*_{EX} in the external part of portion AC of the rod is expressed as (Fig. 1)

$$U^*_{\mathrm{EX}} = \int_{l_1+l_2}^{l_1+l_2+a_2} \int_{R_2}^{R_3} \int_0^{2\pi} u^*_{0\mathrm{EX}} R\mathrm{d}x\mathrm{d}R\mathrm{d}\varphi, \tag{20}$$

(20) where the complementary strain energy density $u^*_{0\mathrm{EX}}$ is determined by replacing of γ with γ_{EX} in Eq. (10). The distribution of the shear strain γ_{EX} in the cross-section of the external part of the rod in portion AC is written as

$$\gamma_{\mathrm{EX}} = \gamma_{\mathrm{mEX}} \frac{R}{R_3}, \tag{21}$$

where

$$R_2 \leq R \leq R_3. \tag{22}$$

The shear strain γ_{mEX} at the periphery of the rod is found by using the following equation for equilibrium (Fig. 1):

$$T_3 = \int_{R_2}^{R_3} \int_0^{2\pi} \tau_{\mathrm{EX}} R^2 \mathrm{d}R\mathrm{d}\varphi, \tag{23}$$

where the distribution of the shear stresses τ_{EX} is obtained by replacing of γ with γ_{EX} in (8). After substituting τ_{EX} in (23), the equation for equilibrium is solved with respect to γ_{EX} by using the MatLab computer program.
The complementary strain energy U^*_{IN2} in the internal part of portion BC of the rod is expressed as (Fig. 1)

$$U^*_{\mathrm{IN2}} = \int_{l_1+a_1}^{l_1+l_2+a_2} \int_0^{R_2} \int_0^{2\pi} u^*_{0\mathrm{IN2}} R\mathrm{d}x\mathrm{d}R\mathrm{d}\varphi, \tag{24}$$

where the complementary strain energy density $u^*_{0\mathrm{IN2}}$ is determined by Eq. (10). For this purpose, γ is replaced with γ_{IN2}. The distribution of the shear strain γ_{IN2} is written as

$$\gamma_{\mathrm{IN2}} = \gamma_{\mathrm{mIN2}} \frac{R}{R_2}, \tag{25}$$

where

$$0 \leq R \leq R_2. \tag{26}$$

The equation for equilibrium that is used to determine the shear strain γ_{mIN2} at the periphery of the internal part of the rod in portion BC is expressed as

$$T_{\mathrm{IN2}} = \int_0^{R_2} \int_0^{2\pi} \tau_{\mathrm{IN2}} R^2 \mathrm{d}R\mathrm{d}\varphi, \tag{27}$$

where T_{IN2} and τ_{IN2} are, respectively, the torsion moment and the shear stresses in the internal portion of the rod. By using Fig. 1, the torsion moment is found as

$$T_{\mathrm{IN2}} = T_2 - T_1. \tag{28}$$

The shear stresses τ_{IN2} are found by replacing of γ with γ_{IN2} in Eq. (8). After substituting of τ_{IN2} and (28) in (27)), the equation for equilibrium is solved with respect to γ_{mIN2} by using the MatLab computer program.
The complementary strain energy U^*_{CD} in the un-cracked portion CD of the rod is expressed as (Fig. 1)

$$U^*_{CD} = \int_{l_1+l_2+a_2}^{l} \int_0^{R_3} \int_0^{2\pi} u^*_{0\mathrm{CD}} R\mathrm{d}x\mathrm{d}R\mathrm{d}\varphi, \tag{29}$$

where the complementary strain energy density $u^*_{0\mathrm{CD}}$ is determined by applying Eq. (10). For this purpose γ is replaced with γ_{CD}. The distribution of the shear stains γ_{CD} is obtained as

$$\gamma_{\mathrm{CD}} = \gamma_{\mathrm{mCD}} \frac{R}{R_3}, \tag{30}$$

where

$$0 \le R \le R_3. \tag{31}$$

In (30) γ_{mCD} is the shear strain at the periphery of the rod in portion CD. The following equation for equilibrium is used to determine γ_{mCD}:

$$T_{\mathrm{CD}} = \int_0^{R_3} \int_0^{2\pi} \tau_{\mathrm{CD}} R^2 \mathrm{d}R\mathrm{d}\varphi, \tag{32}$$

where T_{CD} and τ_{CD} are, respectively, the torsion moment and the shear stresses in the un-cracked portion of the rod. The torsion moment is obtained as (Fig. 1)

$$T_{\mathrm{CD}} = T_1 + T_3 - T_2. \tag{33}$$

The shear stresses τ_{CD} are obtained by replacing of γ with γ_{CD} in (7). After substituting of τ_{CD} and (33) in (32), the equation for equilibrium is solved with respect to γ_{mCD} by using the MatLab computer program.
The following expression for the strain energy release rate is obtained by substituting of (4), (5), (16), (20), (24), (29) in (3):

$$G_{a_1} = \frac{1}{2\pi R_1} \left(\int_0^{R_1} \int_0^{2\pi} u^*_{0\mathrm{IN1}} R\mathrm{d}R\mathrm{d}\varphi + \int_{R_1}^{R_2} \int_0^{2\pi} u^*_{0\mathrm{IS1}} R\mathrm{d}R\mathrm{d}\varphi - \int_0^{R_2} \int_0^{2\pi} u^*_{0\mathrm{IN2}} R\mathrm{d}R\mathrm{d}\varphi \right). \tag{34}$$

The integration in (34) is carried-out by the MatLab computer program.
The strain energy release rate is derived also assuming an elementary increase $\mathrm{d}a_2$ of the length of the external crack (Fig. 1). For this purpose, Eq. (3) is re-written as

$$G_{a_2} = \frac{\mathrm{d}U^*}{2\pi R_2 \mathrm{d}a_2}. \tag{35}$$

In (35) it is taken into account that the length of the front of the external crack is $2\pi R_2$ (Fig. 1). By substituting of (4), (5), (16), (20), (24), (29) in (35), one derives

$$G_{a_2} = \frac{1}{2\pi R_2} \left(\int_{R_2}^{R_3} \int_0^{2\pi} u^*_{0\mathrm{EX}} R\mathrm{d}R\mathrm{d}\varphi + \int_0^{R_2} \int_0^{2\pi} u^*_{0\mathrm{IN2}} R\mathrm{d}R\mathrm{d}\varphi - \int_0^{R_3} \int_0^{2\pi} u^*_{0\mathrm{CD}} R\mathrm{d}R\mathrm{d}\varphi \right). \tag{36}$$

The integration in (36) is performed by the MatLab computer program.
The longitudinal fracture behaviour of the inhomogeneous stepped rod is analyzed also for the case when the external crack is shorter than the internal one (Fig. 2). In portion AB the rod is divided by the two cracks in internal, interstitial and external parts.

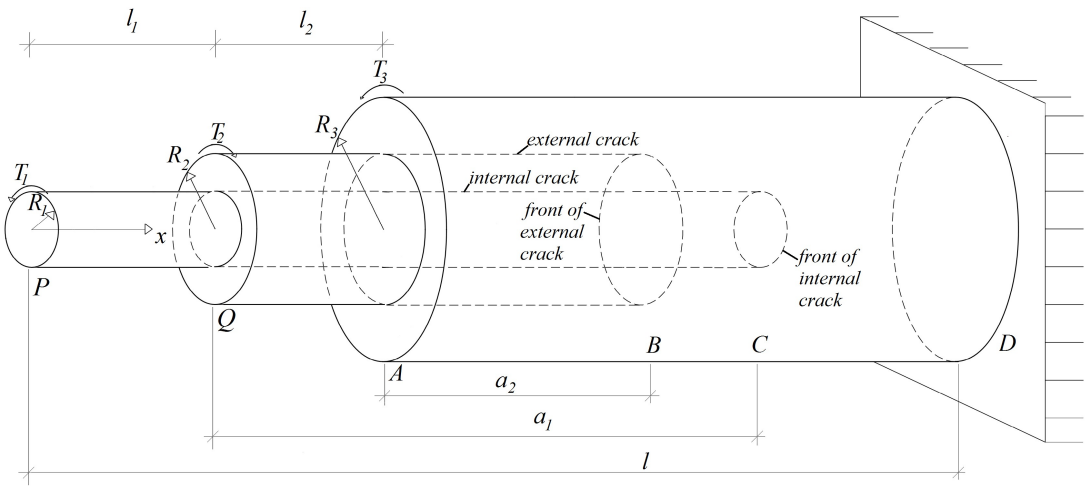

Fig. 2: Inhomogeneous stepped rod configuration in which the external crack is shorter than the internal one

The internal crack divides the portion BC of the rod in internal and external parts. Thus, the complementary strain energy in the rod is expressed as

$$U^* = U^*_{\mathrm{IN1}} + U^*_{\mathrm{IS1}} + U^*_{\mathrm{EX1}} + U^*_{\mathrm{EX2}} + U^*_{\mathrm{CD}}, \tag{37}$$

where U^*_{IN1} is the complementary strain energy in the rod portion PQ and in the internal parts of portions QA and AC of the rod, U^*_{IS1} is the complementary strain energy in the external part of the rod portion QA and in the interstitial part of the portion AB of the rod, U^*_{EX1} is the complementary strain energy in the external part of portion AB of the rod, U^*_{EX2} is the complementary strain energy in the external part of portion BC of the rod, U^*_{CD} is the complementary strain energy in the un-cracked portion CD of the rod.
The complementary strain energy U^*_{IN1} is found by Eq. (5). The complementary strain energy U^*_{IS1} is expressed by Eq. (5). For this purposea_1 is replaced with a_2. The complementary strain energy U^*_{EX1} is obtained by Eq. (20).
The complementary strain energy U^*_{EX2} in the external part of portion BC of the rod is written as

$$U^*_{\mathrm{EX2}} = \int\limits_{l_1+l_2+a_2}^{l_1+a_1} \int\limits_{R_1}^{R_3} \int\limits_{0}^{2\pi} u^*_{0\mathrm{EX2f}} R \mathrm{d}x \mathrm{d}R \mathrm{d}\varphi. \tag{38}$$

Equation (10) is applied to obtain the complementary strain energy density $u^*_{0\mathrm{EX2f}}$. For this purpose γ is replaced with γ_{EX2f}. The distribution of the shear strains γ_{EX2f} is written as

$$\gamma_{\mathrm{EX2f}} = \gamma_{\mathrm{mEX2f}} \frac{R}{R_3}, \tag{39}$$

where

$$R_1 \leq R \leq R_3. \tag{40}$$

The shear strain γ_{mEX2f} at the periphery of the rod in portion BC is found from the following equation for equilibrium:

$$T_{\mathrm{EX2f}} = \int\limits_{R_1}^{R_3} \int\limits_{0}^{2\pi} \tau_{\mathrm{EX2f}} R^2 \mathrm{d}R \mathrm{d}\varphi, \tag{41}$$

where the torsion moment T_{EX2f} is written as (Fig. 2)

$$T_{\mathrm{EX2f}} = T_3 - T_2. \tag{42}$$

The shear stresses τ_{EX2f} are obtained by replacing of γ with γ_{EX2f} in (8). After substituting of τ_{EX2f} and (42) in (41), the equation for equilibrium is solved with respect to γ_{mEX2f} by the MatLab computer program.
Equation (29) is used to derive the complementary strain energy U^*_{CD} in the un-cracked portion CD of the rod. For this purpose a_2 is replaced with a_1.
By substituting of $U^*_{\mathrm{IN1}}, U^*_{\mathrm{IS1}}, U^*_{\mathrm{EX1}}, U^*_{\mathrm{CD}}$, (37) and (38) in (3), one obtains

$$G_{a_1} = \frac{1}{2\pi R_1} \left(\int\limits_{0}^{R_1} \int\limits_{0}^{2\pi} u^*_{0\mathrm{IN1}} R \mathrm{d}R \mathrm{d}\varphi + \int\limits_{R_1}^{R_3} \int\limits_{0}^{2\pi} u^*_{0\mathrm{EX2f}} R \mathrm{d}R \mathrm{d}\varphi - \int\limits_{R_1}^{R_3} \int\limits_{0}^{2\pi} u^*_{0\mathrm{EX2f}} R \mathrm{d}R \mathrm{d}\varphi \right). \tag{43}$$

The integration in (34) is carried-out by using the MatLab computer program.
The strain energy release rate is obtained also assuming an elementary increase da_2 of the external crack in the rod shown in Fig. 2. By substituting of $U^*_{IN1}, U^*_{IS1}, U^*_{EX1}, U^*_{CD}$, (37) and (38) in (35), one derives

$$G_{a_2} = \frac{1}{2\pi R_2}\left(\int\limits_{R_1}^{R_2}\int\limits_{0}^{2\pi} u^*_{0IS1} R\mathrm{d}R\mathrm{d}\varphi + \int\limits_{R_2}^{R_3}\int\limits_{0}^{2\pi} u^*_{0EX} R\mathrm{d}R\mathrm{d}\varphi - \int\limits_{R_1}^{R_3}\int\limits_{0}^{2\pi} u^*_{0EX2f} R\mathrm{d}R\mathrm{d}\varphi\right). \tag{44}$$

The MatLab computer program is used to perform the integration in (4).

2.2 Calculation of the strain energy release rate by considering the energy balance

For verification, the strain energy release rates are derived also by considering the balance of the energy. First, the stepped rod shown in Fig. 1 is analyzed. By assuming a small increase δa_1 of the length of the internal crack, the balance of the energy is written as

$$T_1\delta\psi_1 + T_2\delta\psi_2 + T_3\delta\psi_3 = \frac{\partial U}{\partial a_1}\delta a_1 + G_{a_1} l_{cf1}\delta a_1, \tag{45}$$

where ψ_1, ψ_2 and ψ_3 are, respectively, the angles of twist of the cross-sections P, Q and A of the rod, U is the strain energy stored in the rod. By combining of (2) and (45), one derives

$$G_{a_1} = \frac{T_1}{2\pi R_1}\frac{\partial\psi_1}{\partial a_1} + \frac{T_2}{2\pi R_1}\frac{\partial\psi_2}{\partial a_1} + \frac{T_3}{2\pi R_1}\frac{\partial\psi_3}{\partial a_1} - \frac{1}{2\pi R_1}\frac{\partial U}{\partial a_1}. \tag{46}$$

The angles of twist ψ_1, ψ_2 and ψ_3 are obtained by the integrals of Maxwell-Mohr. The result is

$$\begin{aligned}
\psi_1 &= \frac{\gamma_m}{R_1}(l_1 + a_1) + \frac{\gamma_{mIN2}}{R_2}(a_2 - a_1 + l_2) + \frac{\gamma_{mCD}}{R_3}(l - a_2 - l_1 - l_2),\\
\psi_2 &= \frac{\gamma_{mIN1}}{R_2}a_1 + \frac{\gamma_{mIN2}}{R_2}(a_2 - a_1 + l_2) + \frac{\gamma_{mCD}}{R_3}(l - a_2 - l_1 - l_2),\\
\psi_3 &= \frac{\gamma_{mEX}}{R_3}a_2 + \frac{\gamma_{mCD}}{R_3}(l - a_2 - l_1 - l_2).
\end{aligned} \tag{47}$$

The strain energy in the rod is written as

$$U = U_{IN1} + U_{IS1} + U_{EX} + U_{IN2} + U_{CD}, \tag{48}$$

where U_{IN1} the complementary strain energy in the rod portion PQ and in the internal parts of portions QA and AB of the rod, U_{IS1} is the complementary strain energy in the external part of the rod portion QA and in the interstitial part of the portion AB of the rod, U_{EX} is the complementary strain energy in the external part of portion AC of the rod, U_{IN2} is the complementary strain energy in the internal part of portion BC of the rod, U_{CD} is the complementary strain energy in the un-cracked portion CD of the rod. Equation (5) is used to determine U_{IN1}. For this purpose u^*_{0IN1} is replaced with u_{0IN1}. The strain energy U_{IS1} is obtained by replacing of u^*_{0IS1} with u_{0IS1} in Eq. (16). The strain energy density is found by (9). For this purpose γ is replaced with γ_{IN1}. Equation (20) is applied to obtain U_{EX}. For this purpose u^*_{0EX} is replaced with u_{0EX}, where u_{0EX} is found by replacing of γ with γ_{EX} in (9). The strain energy U_{IN2} is found by replacing of u^*_{0IN2} with u_{0IN2} in (24). The strain energy density u_{0IN2} is obtained by replacing of γ with γ_{IN2} in (9). Equation (29) is used to determine U_{CD} by replacing of u^*_{0CD} with u_{0CD}. Equation (9) is applied to obtain the strain energy density u_{0CD}. For this purpose γ is replaced with γ_{CD}.
By substituting of $U_{IN1}, U_{IS1}, U_{EX}, U_{IN2}, U_{CD}$, (47) and (48) in (46), one derives

$$\begin{aligned}
G_{a_1} &= \frac{T_1}{2\pi R_1}\left(\frac{\gamma_m}{R_1} - \frac{\gamma_{mIN2}}{R_2}\right) + \frac{T_2}{2\pi R_1}\left(\frac{\gamma_{mIN1}}{R_2} - \frac{\gamma_{mIN2}}{R_2}\right)\\
&- \frac{1}{2\pi R_1}\left(\int\limits_{0}^{R_1}\int\limits_{0}^{2\pi} u_{0IN1} R\mathrm{d}R\mathrm{d}\varphi + \int\limits_{R_1}^{R_2}\int\limits_{0}^{2\pi} u_{0IS1} R\mathrm{d}R\mathrm{d}\varphi - \int\limits_{0}^{R_2}\int\limits_{0}^{2\pi} u_{0IN2} R\mathrm{d}R\mathrm{d}\varphi\right)
\end{aligned} \tag{49}$$

The integration in (49) is carried-out by the MatLab computer program. The fact that the strain energy release rate obtained by (49) matches exactly that found by (34) is a verification of analysis carried-out assuming increase of the internal crack in the rod shown in Fig. 1.
The strain energy release rate is obtained also assuming a small increase δa_2 of the length of the external crack in the rod shown in Fig. 1. For this purpose, (46) is re-written as

$$G_{a_2} = \frac{T_1}{2\pi R_2}\frac{\partial\psi_1}{\partial a_2} + \frac{T_2}{2\pi R_2}\frac{\partial\psi_2}{\partial a_2} + \frac{T_3}{2\pi R_2}\frac{\partial\psi_3}{\partial a_2} - \frac{1}{2\pi R_2}\frac{\partial U}{\partial a_2}. \tag{50}$$

By substituting of $U_{IN1}, U_{IS1}, U_{EX}, U_{IN2}, U_{CD}$, (47) and (48) in (50), one obtains

$$\begin{aligned} G_{a_2} &= \frac{T_1}{2\pi R_2}\left(\frac{\gamma_{mIN}}{R_1}-\frac{\gamma_{mCD}}{R_3}\right)+\frac{T_2}{2\pi R_2}\left(\frac{\gamma_{mIN2}}{R_2}-\frac{\gamma_{mCD}}{R_3}\right) \\ &- \frac{1}{2\pi R_2}\left(\int_{R_2}^{R_3}\int_0^{2\pi} u_{0EX}R\mathrm{d}R\mathrm{d}\varphi+\int_0^{R_2}\int_0^{2\pi} u_{0IN2}R\mathrm{d}R\mathrm{d}\varphi-\int_0^{R_3}\int_0^{2\pi} u_{0CD}R\mathrm{d}R\mathrm{d}\varphi\right) \end{aligned} \tag{51}$$

The MatLab computer program is used to carry-out the integration in (51). The strain energy release rate obtained by (51) is exact of that found by (36). This fact is a verification of analysis carried-out assuming increase of the external crack in the rod shown in Fig. 1.

The solutions to the strain energy release rate for the case when the external crack is shorter than the internal one are also verified. For this purpose, the strain energy in the rod shown in Fig. 2 is written as

$$U = U_{IN1} + U_{IS1} + U_{EX1} + U_{EX2} + U_{CD}, \tag{52}$$

where U_{IN1} is the complementary strain energy in the rod portion PQ and in the internal parts of portions QA and AC of the rod, U_{IS1} is the complementary strain energy in the external part of the rod portion QA and in the interstitial part of the portion AB of the rod, U_{EX1} is the complementary strain energy in the external part of portion AB of the rod, U_{EX2} is the complementary strain energy in the external part of portion BC of the rod, U_{CD} is the complementary strain energy in the un-cracked portion CD of the rod.

The strain energy U_{IN1} is obtained by replacing of u^*_{0IN1} with u_{0IN1} in (5). The strain energy U_{IS1} is found by replacing of a_1 and u^*_{0IS1} with a_2 and u_{0IS1} in Eq. (16). The strain energy U_{EX1} is obtained by replacing of u^*_{0EX} with u_{0EX} in Eq. (20). The strain energy U_{EX2} in the external part of portion BC of the rod is found by replacing of u^*_{0EX2f} with u_{0EX2f} in (38). The strain energy density u_{0EX2f} is obtained by replacing of γ with γ_{EX2f} in (9). Equation (29) is applied to derive the strain energy U_{CD} in the un-cracked portion CD of the rod. For this purpose a_2 and u^*_{0CD} are replaced with a_1 and u_{0CD}, respectively.

By using the integrals of Maxwell-Mohr, the angles of twist of the free ends of the internal, interstitial and external parts of the rod are written as (Fig. 2)

$$\begin{aligned} \psi_1 &= \frac{\gamma_m}{R_1}(l_1+a_1)+\frac{\gamma_{mCD}}{R_3}(l-a_1-l_1), \\ \psi_2 &= \frac{\gamma_{mIN1}}{R_2}(l_2+a_2)+\frac{\gamma_{mEX2f}}{R_3}(a_1-a_2-l_2)+\frac{\gamma_{mCD}}{R_3}(l-a_1-l_1), \\ \psi_3 &= \frac{\gamma_{mEX}}{R_3}a_2+\frac{\gamma_{mEX}2f}{R_3}(a_1-a_2-l_2)+\frac{\gamma_{mCD}}{R_3}(l-a_1-l_1). \end{aligned} \tag{53}$$

First, a small increase δa_1 of the length of the internal crack is assumed (Fig. 2). Thus, by substituting of $U_{IN1}, U_{IS1}, U_{EX1}, U_{EX2}, U_{CD}$, (52), (53) in (46), one arrives at

$$\begin{aligned} G_{a_1} &= \frac{T_1}{2\pi R_1}\left(\frac{\gamma_m}{R_1}-\frac{\gamma_{mCD}}{R_3}\right)+\frac{T_2}{2\pi R_1}\left(\frac{\gamma_{mEX2f}}{R_3}-\frac{\gamma_{mCD}}{R_3}\right) \\ &- \frac{1}{2\pi R_1}\left(\int_0^{R_1}\int_0^{2\pi} u_{0IN1}R\mathrm{d}R\mathrm{d}\varphi+\int_{R_1}^{R_3}\int_0^{2\pi} u_{0EX2}R\mathrm{d}R\mathrm{d}\varphi-\int_0^{R_1}\int_0^{2\pi} u_{0CD}R\mathrm{d}R\mathrm{d}\varphi\right) \end{aligned} \tag{54}$$

The integration in (54) is carried-out by the MatLab computer program. It should be noted that the strain energy release rate obtained by (54) is exact match of that found by (43).

The strain energy release rate for the rod shown in Fig. 2 is derived also assuming a small increase δa_2 of the length of the external crack. By substituting of $U_{IN1}, U_{IS1}, U_{EX1}, U_{EX2}, U_{CD}$, (52) and (53) in (50), one obtains

$$\begin{aligned} G_{a_2} &= \frac{T_2}{2\pi R_2}\left(\frac{\gamma_{mIN}1}{R_2}-\frac{\gamma_{mEX2f}}{R_3}\right)+\frac{T_3}{2\pi R_2}\left(\frac{\gamma_{mEX}}{R_3}-\frac{\gamma_{mEX2f}}{R_3}\right) \\ &- \frac{1}{2\pi R_2}\left(\int_{R_1}^{R_2}\int_0^{2\pi} u_{0IS1}R\mathrm{d}R\mathrm{d}\varphi+\int_{R_2}^{R_3}\int_0^{2\pi} u_{0EX}R\mathrm{d}R\mathrm{d}\varphi-\int_{R_1}^{R_3}\int_0^{2\pi} u_{0EX2}R\mathrm{d}R\mathrm{d}\varphi\right) \end{aligned} \tag{55}$$

The MatLab computer program is used to perform the integration in (55). The fact that the strain energy release rate found by (55) is exact match of that obtained by (44) is a verification of the fracture analysis carried-out assuming increase of the external crack in the stepped rod in Fig. 2.

3 Results and discussion

In this section, the solutions to the strain energy release rate derived in the previous section of the paper are used to investigate the influence of various geometrical parameters and material inhomogeneity on the longitudinal fracture behaviour of the stepped rod

with two concentric longitudinal cracks. The strain energy release rate is presented in non-dimensional form by using the formula $G_N = G_{a_1}/(G_0 R_3)$. It is assumed that $T_1 = 5$ Nm, $T_2 = 8$ Nm, $T_3 = 7$ Nm, $R_3 = 0.010$ m and $l = 0.500$ m.

The influence of the location of the internal crack in radial direction on the fracture behaviour is analyzed. The rod shown in Fig. 1 is considered. The location of the internal crack is characterized by R_1/R_3 ratio. The influence of the location of the internal crack on the fracture is illustrated in Fig. 3, where the strain energy release rate in non-dimensional form is presented as a function of R_1/R_3 ratio at $R_2/R_3 = 0.8$. The curves shown in Fig. 3 indicate that the strain energy release rate increases with increasing of R_1/R_3 ratio. One can observe also in Fig. 3 that the strain energy release rate derived assuming increase of external crack is higher than that obtained assuming increase of the internal crack.

The influence of the material property p on the fracture behaviour is analyzed too. The rod in which the external crack is shorter than the internal one is under consideration (Fig. 1). The solution to the strain energy release rate derived assuming increase of the external crack is applied. One can get an idea about the influence of p on the fracture in Fig. 4 where the strain energy release rate in non-dimensional form is presented as a function of at three R_2/R_3 ratios for $R_1/R_3 = 0.2$ (the ratio R_2/R_3 characterizes the location of the external crack in radial direction).

It can be observed in Fig. 4 that the strain energy release rate decreases with increasing of p. This finding is attributed to the fact that the stiffness of the rod increases with increasing of p. The curves in Fig. 4 indicate that the strain energy release rate increases with increasing of R_2/R_3 ratio.

The longitudinal fracture behaviour is analyzed also for the case when the rod exhibits continuous (smooth) material inhomogeneity in both radial and length directions. The distribution of G_0 along the length of the rod is written as

$$G_0 = G_{0b} e^{q\frac{x}{l}}, \tag{56}$$

where

$$0 \le x \le l. \tag{57}$$

In (56) G_{0b} is the value of G_0 at the free end of the rod, q is a material property that controls the material inhomogeneity in the length direction. When the rod is inhomogeneous in radial and length directions, the strain energy release rate can be obtained by applying the solutions derived in the previous section of the paper. For this purpose, the material property G_0 has to be calculated by (56) for the corresponding crack length. The effect of q on the fracture behaviour is illustrated in Fig. 5 where the strain energy release rate in non-dimensional form is presented as a function of q at $a_2/(l - l_1 - l_2) = 0.4$ (the solutions to the strain energy release rate obtained at increase of the external crack in the rods shown in Figs. 1 and 2 are applied). It is evident from Fig. 5 that the strain energy release rate decreases with increasing of q (this behaviour is due to the increase of the stiffness of the rod). The curves in Fig. 5 show also that the strain energy release rate is higher in the stepped rod configuration in which the external crack is shorter (Fig. 2). This finding can be explained by the fact that when the external crack is shorter, the crack front is located in cross-section of the rod in which the stiffness is lower since the stiffness increases from the free end of the rod towards the clamping according to (56).

4 Conclusions

The longitudinal fracture behavior of an inhomogeneous stepped rod with two longitudinal concentric cracks is analyzed in terms of the strain energy release rate. The rod has a circular cross-section. The two concentric longitudinal cracks present circular cylindrical surfaces. The rod under consideration exhibits continuous (smooth) material inhomogeneity in radial direction. Besides, the material has non-linear elastic behaviour. The rod is loaded in torsion. Solutions to the strain energy release rate are derived at different lengths of the two cracks by considering the complementary strain energy stored in the rod. The solutions are verified by analyzing the balance of the energy. It is shown that the solutions can be applied also for stepped rods which exhibit continuous

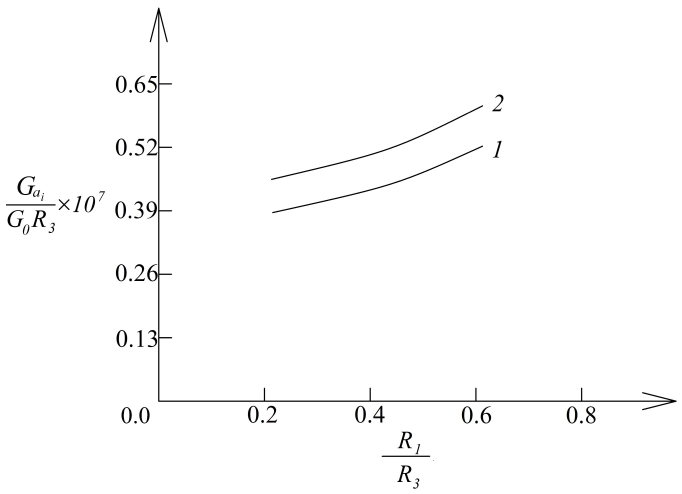

Fig. 3: The strain energy release rate in non-dimensional form presented as a function of R_1/R_3 ratio (curve 1 – at increase of the internal crack and curve 2 – at increase of the external crack)

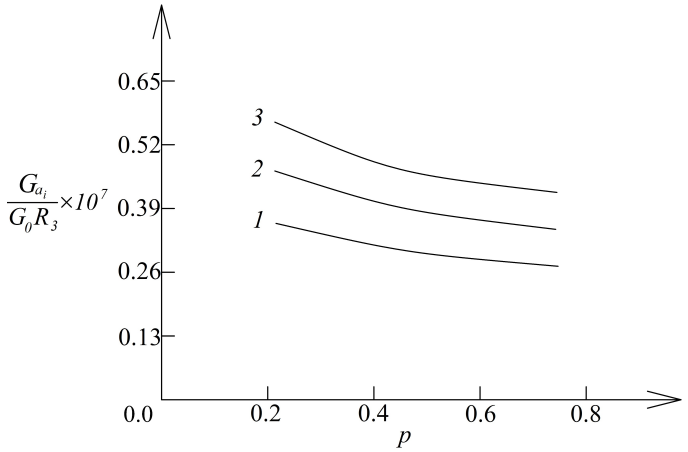

Fig. 4: The strain energy release rate in non-dimensional form presented as a function of p (curve 1 – at $R_2/R_3 = 0.3$, curve 2 – at $R_2/R_3 = 0.5$ and curve 3 – at $R_2/R_3 = 0.7$)

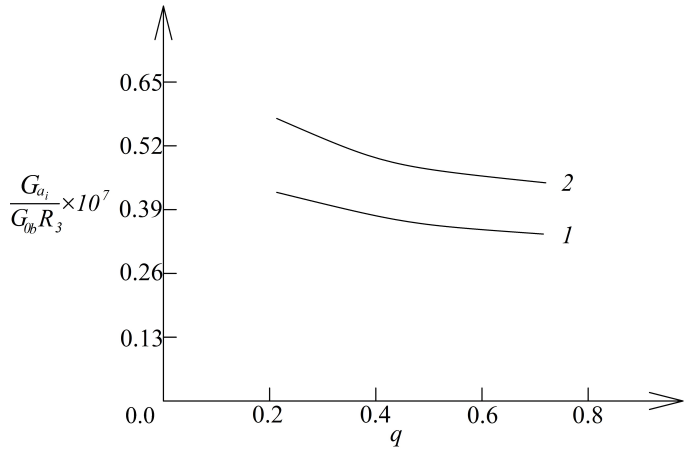

Fig. 5: The strain energy release rate in non-dimensional form presented as a function of q (curve 1 – for the stepped rod shown in Fig. 1 and curve 2 – for the stepped rod in which the external crack is shorter (Fig.2))

material inhomogeneity in both radial and length directions. The influence of the locations of the two cracks in radial direction on the fracture behaviour is investigated. It is found that the strain energy release rate increases with increasing of R_1/R_3 ratio. The increase of R_2/R_3 ratio leads also to increase of the strain energy release rate. The analysis reveals that the strain energy release rate decreases with increasing of material property p. It is found also that the strain energy release rate obtained at increase of external crack is higher than that obtained at increase of the internal crack. Concerning the effect of material inhomogeneity along the length of the rod, it is found that the strain energy release rate decreases with increasing of material property q. The analysis indicates also that the strain energy release rate is higher in the stepped rod in which the external crack is shorter.

Acknowledgement

The first author (V.R.) gratefully acknowledges the financial support by the German Academic Exchange Service (DAAD) for his research stay at the Chair of Engineering Mechanics, Institute of Mechanics, Otto-von-Guericke-Universität Magdeburg, Germany.

References

Erkin Altunsaray and Ismail Bayer. Buckling of symmetrically laminated quasi-isotropic thin rectangular plates. *Steel and Composite Structures*, 17(3):305–320, 2014.

Alberto Carpinteri and Nicola Pugno. Cracks and re-entrant corners in functionally graded materials. *Engineering Fracture Mechanics*, 73(10):1279 – 1291, 2006.

F. Erdogan. Fracture mechanics of functionally graded materials. *Composites Engineering*, 5(7):753 – 770, 1995.

D.K. Jha, Tarun Kant, and R.K. Singh. A critical review of recent research on functionally graded plates. *Composite Structures*, 96:833 – 849, 2013.

G.E. Knoppers, J.W. Gunnink, J. van den Hout, and W.P. van Vliet. The reality of functionally graded material products. *TNO Science and Industry*, pages 38 – 43, 2003.

P. A. Lukash. *Fundamentals of non-linear structural mechanics*. Stroizdat, Moscow, 1998.

R.M. Mahamood and E.T. Akinlabi. *Functionally Graded Materials*. Springer, 2017.

Y. Miyamoto, W.A. Kaysser, B.H. Rabin, A. Kawasaki, and R.G. Ford. *Functionally Graded Materials: Design, Processing and Applications*. Kluwer Academic Publishers, Dordrecht/London/Boston, 1999.

M.M. Nemat-Allal, M.H. Ata, M.R. Bayoumi, and W. Khair-Eldeen. Powder metallurgical fabrication and microstructural investigations of aluminum/steel functionally graded material. *Materials Sciences and Applications*, 2(12):1708–1718, 2011.

G.H. Paulino. Fracture of functionally graded materials. *Engineering Fracture Mechanics*, 69(14–16):1519–1530, 2002.

V. Rizov. Multilayered functionally graded non-linear elastic beams with logarithmic material gradient: A delamination analysis. *Technische Mechanik*, 38(2):203–219, 2018.

Matthew T. Tilbrook, Robert J. Moon, and Mark Hoffman. Crack propagation in graded composites. *Composites Science and Technology*, 65(2):201–220, 2005.

L. Tokova, A. Yasinskyy, and C.-C Ma. Effect of the layer inhomogeneity on the distribution of stresses and displacements in an elastic multilayer cylinder. *Acta Mechanica*, 228(8):2865—-2877, 2017.

Y. Tokovyy and C.-C. Ma. Analysis of 2D non-axisymmetric elasticity and thermoelasticity problems for radially inhomogeneous hollow cylinders. *Journal Engineering Mathematics*, 61(2–4):171–184, 2008.

Y. Tokovyy and C.-C. Ma. Three-dimensional temperature and thermal stress analysis of an inhomogeneous layer. *Journal of Thermal Stresses*, 36(8):790–808, 2013.

Y. Tokovyy and C.-C. Ma. Axisymmetric stresses in an elastic radially inhomogeneous cylinder under length-varying loadings. *ASME Journal of Applied Mechanics*, 83(11):111007 (7 pages), 2016.

M.U. Uysal. Buckling behaviours of functionally graded polymeric thin-walled hemispherical shells. *Steel and Composite Structures*, 21(4):849–862, 2016.

M.U. Uysal and U. Güven. A bonded plate having orthotropic inclusion in the adhesive layer under in-plane shear loading. *The Journal of Adhesion*, 92(3):214–235, 2016.

M.U. Uysal and M. Kremzer. Buckling behaviour of short cylindrical functionally gradient polymeric materials. *Acta Physica Polonica A*, 127(4):1355–1357, 2017.